Catal Lett (2008) 120:86–94
DOI 10.1007/s10562-007-9253-z

Effect of CeO_2 and La_2O_3 on the Activity of CeO_2–La_2O_3/Al_2O_3-Supported Pd Catalysts for Steam Reforming of Methane

W. H. Cassinelli · L. S. F. Feio · J. C. S. Araújo · C. E. Hori · F. B. Noronha · C. M. P. Marques · J. M. C. Bueno

Received: 1 August 2007 / Accepted: 24 August 2007 / Published online: 11 September 2007

Abstract The effect of the addition of CeO_2 or La_2O_3 on the surface properties and catalytic behaviors of Al_2O_3-supported Pd catalysts was studied in the steam reforming of methane. The FTIR spectroscopy of adsorbed CO and the Pd dispersion suggest the partial coverage of Pd^0 by ceria or lanthana species. This could lead to the formation of an adduct MPd_xO (M = Ce or La) at the surface of the metal crystallites. The addition of ceria or lanthana resulted in an increase of the turnover rate and specific rate for steam reforming of methane. One possible explanation if that the Pd^0*$Pd^{\delta+}$O–M interfacial species (M = Ce or La) are oxidized by H_2O or CO_2, promoting the O* transfer to the metal surface. This could facilitate the removal of C* species from the metal surface, resulting in the increase of specific reaction rate and increase of the accessibility of CH_4 to metal active sites.

Keywords Pd catalysts · La_2O_3–Al_2O_3 carriers · CeO_2–Al_2O_3 carriers · Steam reforming of methane · XRD · TPR · FTIR

W. H. Cassinelli · C. M. P. Marques
DQ, Universidade Federal de São Carlos, C.P. 676, Sao Carlos, SP 13565-905, Brazil

L. S. F. Feio · J. C. S. Araújo · J. M. C. Bueno (✉)
DEQ, Universidade Federal de São Carlos, C.P. 676, Sao Carlos, SP 13565-905, Brazil
e-mail: jmcb@power.ufscar.br

C. E. Hori
FEQ, Universidade Federal de Uberlândia, Uberlandia, MG, Brazil

F. B. Noronha
Instituto Nacional de Tecnologia - INT, Rio de Janeiro, RJ, Brazil

1 Introduction

Throughout the centuries, different energy sources have been used to power the development of mankind. Recently, the use of hydrogen as a clean and possibly renewable energy source has been drawing a lot of attention from researchers and governmental agencies all around the world. The most studied technology for hydrogen production from fossil fuels is steam-methane reforming (SMR). In this route, methane reacts with steam to produce a mixture of hydrogen, carbon dioxide, and carbon monoxide. The industrial processes use supported Ni catalysts with Ni loadings around 12 wt.%. However, Ni-based catalysts are active to the formation of carbon filaments and it is susceptive to the oxidation by water. Alternatively, noble metal-based catalysts are more active, are more dispersed on support and less susceptible to carbon formation. These properties can minimize their high cost and therefore, they can become versatile to different applications of hydrocarbon reforming [1–3].

In order to obtain catalysts with high activity and stability, it is fundamental to avoid the sintering processes to maintain the dispersion of the active phase and the support stability [1]. Both properties are considered to be crucial to achieve good catalytic performance for the steam reforming of methane. Lanthana dispersed on alumina is a system of considerable interest for reforming methane because La_2O_3 is able to stabilize transition alumina and it can also avoid Pt agglomeration [4]. The widespread use of ceria as a promoter started with the automotive applications. Nowadays, its special properties such as oxygen storage capacity, improvement of metal dispersions and good activity for water gas shift reaction have amplified the use of this material to several different reaction systems. By considering these aspects, the goal of present work is to

study the effect of CeO_2 and La_2O_3 on catalytic properties of supported Pd catalysts in the steam reforming of methane.

2 Experimental

2.1 Catalyst Preparation

The supports with various CeO_2 and La_2O_3 loadings were prepared by impregnation of γ-alumina (S_{BET} = 205 m^2/g) with aqueous solution of $(NH_4)_2[Ce(NO_3)_6]$ or $La(NO_3)_3.6H_2O$. The carriers were prepared with 1, 6 and 12 wt.% of ceria or lanthana on alumina. For all samples, the Pd content was 1.0 wt.% obtained through the wetness impregnation of the supports with an aqueous solution of $Pd(NO_3)_2$. The samples were dried at 333 K overnight and calcined at 773 K for 2 h under air flow. Samples were denoted as Pd/Al_2O_3, Pd/xCe–Al_2O_3, Pd/xLa–Al_2O_3 where x correspond to loading of CeO_2 or La_2O_3.

2.2 Characterization

BET surface areas, S_{BET}, were measured by N_2 adsorption at liquid nitrogen temperature using a Quantachrome Nova model 1200. The samples were initially dried at 473 K for 2 h under vacuum in order to clean the surface. Then the N_2 adsorption was performed at 77 K.

X-ray diffraction (XRD) profiles of the samples were collected using a Rigaku Multiflex diffractometer, using Cu–K_α radiation. The step-scans were taken over the range of 2θ from 10 to 75° in steps of 0.020° and the intensity data for each one were collected for 10 s. The size of the crystallites of ceria was determined using Scherrer equation [5].

Temperature-programmed reduction (TPR) profiles of the samples were recorded on a micro-reactor coupled with a quadrupole mass spectrometer (Omnistar, Balzers). In order to remove the surface contaminants, the sample (0.3 g) loaded in a quartz reactor was pretreated at 423 K in a He stream for 1 h. After cooling to room temperature, a flow of 10% H_2/Ar (30 mL/min) was passed through the sample and the temperature was raised at a rate of 10 K/min up to 1,273 K while the mass spectrometry signal was recorded.

Usually metal dispersions are determined by H_2 or CO chemisorption. However, for palladium supported samples on carriers containing ceria or lanthana, the dispersion values may be incorrect due to adsorption on the supports and the formation of palladium hydride. In order to overcome these problems, an indirect method was used to determine the metal dispersion [6, 7]. The dehydrogenation of cyclohexane is a structure insensitive reaction and therefore its rate is independent of the dispersion of the metal on the surface. This reaction was performed in a fixed-bed reactor at atmospheric pressure and the reaction rate was measured at 673 K. A H_2/Cyclohexane ratio equals to 13 was used, for a 10 mg sample and total gas flow rate of 200 mL/min. Prior to the reaction, the catalysts were reduced at 773 K for 1 h. After this, the samples were cooled to the reaction temperature. The reactor effluent was analyzed using a GC-17A Shimadzu using a FID detector and a Cromopack CP-Wax 57 CB column. The obtained reaction rates were compared to rates obtained for standard samples with known dispersions. The obtained reaction rates were compared to rates obtained for standard samples with known dispersions. The plot dehydrogenation of cyclohexane rates and Pd dispersion for various Pd/Al_2O_3 catalysts, with Pd dispersion at region 10–50%, and linear correlation of 0.9999 was used as standard samples.

X-ray photoemission spectroscopy (XPS) spectra were obtained with an ESCALAB MKII, VG Scientific spectrometer by using a non-monochromatic Al Kα (E = 1486.6 eV) X-ray source. The spectra were collected with pass energy of 50 eV for the high resolution spectra and 100 eV for the survey spectra, and using the electromagnetic lens. The residual pressure inside the analysis chamber was of the order of 10^{-8} mbar. The binding energies (BE) of Pd 4*d*; Ce 3*d*, La 3*d* and O 1*s* were determined by a computer fitting using Spectra V.8 program of the measured spectra and referred to the C 1*s* line at 2,848 eV. The binding energies were estimated to within ± 0.2 eV .

FTIR Spectroscopy for characterization of the surface of Pd particles, the CO adsorption was utilized. The infrared spectra for adsorbed CO were recorded by a FT-IR THERMO NICOLET 4700 NEXUS spectrophotometer with MCT detector and Diffuse Reflectance Infrared Fourier Transform Spectroscopy and reactor cell with CaF_2 windows (DRIFT HTHV cell—Spectra Tech). The samples were pre-reduced at different temperatures under 25% H_2/N_2 mixture for 1 h, before the samples were kept under vacuum at temperature reduction for 5 min. After introduction of N_2 into the cell, the samples were cooled to 298 K. The catalysts were exposure to CO at 298 K and CO pressure of 20 torr.

2.3 Catalytic Test

The rates of steam reforming of CH_4 were measured on catalysts powders (100 mg) diluted with quartz (300 mg) of similar size in a fixed bed quartz reactor at atmospheric pressure and temperature at region 693–713 K. The reaction rate was obtained under differential conditions, the

effect of mass and heat transfer resistances external and/or internal the particles were minimized by applying experimental criteria. Under experimental reaction condition, the water–gas shift reaction is equilibrated and the selectivity to CO_2 was around 100% and similar for all catalyst. The gas composition of the reactants and products were analyzed by the gas chromatograph as previously described elsewhere [8, 9]. Feed composition $CH_4/H_2O/N_2$ was 1:3:2.5 at a total flow rate of 1.3×10^{-2} mol/min. The apparent activation energy (E_a^{ap}) was estimated using non-linear methods from fitting the experimental data to the Ahrrenius equation. The CH_4 turnover rates (TOF_{CH4}) were calculated considering the Pd dispersion obtained in the reaction of cyclohexane dehydrogenation.

3 Results

Textural properties of catalysts with different La_2O_3 and CeO_2 loadings after treatment in air at 773 K are listed in Table 1. Surface area and pore volume of the samples decrease with the increase of La_2O_3 and CeO_2 loadings. For Pd/*x*Ce–Al_2O_3 catalysts the surface area values are identical to that calculated by theoretical physical mixture, while for Pd/*x*La–Al_2O_3 surface area values are lower. Probably the alumina pores are not blocked by CeO_2 agglomeration, and there is a partial pore filling of the alumina by incorporation of the La_2O_3 which blocks the smaller pores.

Pd dispersions of the samples reduced at 773 K determined by dehydrogenation of cyclohexane are also presented in Table 1. The addition of low lanthana loadings (La ≤ 6 wt.%) increases the palladium dispersion, while a decrease of palladium dispersion occurs at higher lanthana loading (La = 12 wt.%). For Ce-containing samples, the palladium dispersions strongly decrease with the addition of ceria to the alumina support. This effect cannot be correlated just to changes of textural properties of the samples. The BET surface area decreased strongly for the La-containing samples, but the Pd dispersions did not. On the other hand, for Pd/*x*Ce–Al_2O_3 samples, the BET surface area and pore volume did not dropped sharply, although the Pd dispersion did. Therefore, this effect will be discussed latter, after the presentation of the FTIR of adsorbed CO data.

The XRD profiles of Pd supported on Al_2O_3, *x*La–Al_2O_3 and *x*Ce–Al_2O_3, calcined at 773 K are shown in Fig. 1. The XRD patterns of La_2O_3 and a Pd/CeO_2 are also shown in order to show the °2θ positions of the main ceria and lanthana peaks. For all the samples, it was possible to observe the diffraction patterns relative to the γ-structure of Al_2O_3 and no bulk La_2O_3 was identified. However, the addition of lanthana caused a sharp decrease on the intensity of the alumina peaks, and this effect is probably

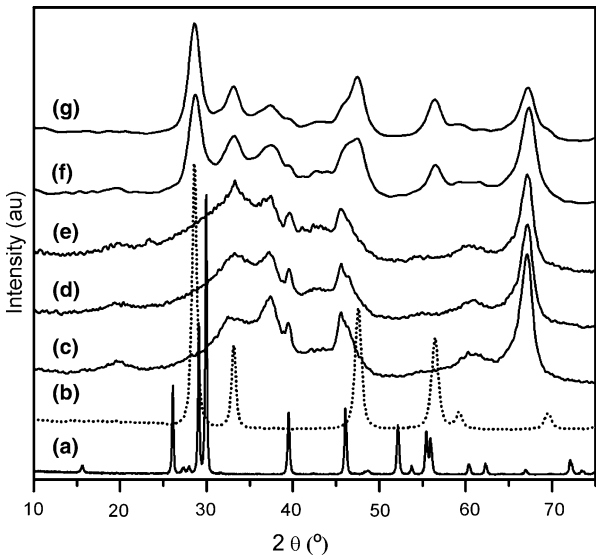

Fig. 1 XRD spectra of La_2O_3 (**a**), Pd/CeO_2 (**b**), Pd/Al_2O_3 (**c**), Pd/6La–Al_2O_3 (**d**), Pd/12La–Al_2O_3 (**e**), Pd/6Ce–Al_2O_3 (**f**) and Pd/12Ce–Al_2O_3 (**g**)

Table 1 Surface area (S_{BET}), pore volume (Vp), Palladium dispersions (D_{Pd}), Steam Reforming of Methane Reaction Rate, Turnover Frequency (TOF) at 783 K and Apparent Activation Energy (E_a^{ap}) for all the catalysts

Catalysts	S_{BET} (m^2/g)	Vp (cm^3/g)	D_{Pd} (%)	H_2cons./PdO *		Rate × 10^{-5} (mol · s^{-1} · g_{cat}^{-1})	E_a^{ap} (kJ/mol)	LF/HF	TOF (s^{-1})
				at r.t.	>300 K				
Pd/Al_2O_3	167	0.23	40	0.17	0.83	2.88	94.1	5.2	0.96
Pd/1La–Al_2O_3	156	0.22	60	0.25	0.77	6.61	87.9	3.2	1.4
Pd/6La–Al_2O_3	106	0.17	57	0.25	0.88	6.72	84.9	2.5	1.6
Pd/12La–Al_2O_3	98	0.13	43	0.21	1.07	8.05	74.8	2.0	2.5
Pd/3Ce–Al_2O_3	166	0.23	27	–	–	3.74	79.1	4.2	1.9
Pd/6Ce–Al_2O_3	159	0.22	25	0.6	1.44	5.07	80.0	3.3	3.2
Pd/12Ce–Al_2O_3	151	0.20	22	0.6	1.63	5.86	73.2	1.7	4.7

* H_2 consumption/PdO ratio at room temperature and at temperatures region higher than 300 K

related to the high radiation absorption capacity of lanthana. Barrera et al. [10] also obtained similar results while studying γ-Al_2O_3 samples promoted with 15 wt. % of La. The authors suggested that the lanthanum atoms are highly dispersed on the alumina structure and the decrease of the intensity is possibly related to the structure disorder of the alumina caused by La after the thermal treatment. Therefore, it may be suggested that lanthanum is either incorporated within the vacancies of the γ-Al_2O_3 structure or it forms small lanthanum oxide particles well dispersed. For the ceria containing samples, one can observe an aggregation of crystalline CeO_2 with increasing ceria loadings. No XRD patterns of PdO species in the precursor samples were observed. These results suggest that a large fraction of Pd particles are well dispersed on the surface of catalysts with different lanthana and ceria loading.

The H_2 uptake during TPR experiments for all the samples are shown in Fig. 2. TPR profile for Pd/Al_2O_3 catalyst displays a peak at room temperature, a small negative peak around 335 K, a large one around 440 K, and a minor peak, poorly resolved, near 650 K. The H_2 consumption at room temperature is usually related to the reduction of large Pd-oxide species and to the formation of palladium hydrate, according to literature data [11]. The small negative peak at 335 K is assigned to the desorption of weakly adsorbed hydrogen from the palladium surface and to the decomposition of the palladium hydrate (β-$PdH_{0,6}$) formed during the initial stages of the reduction process, according to Lieske and Volter [11]. The peak around 440 K may be related to the reduction of small clusters or isolated patches of PdO_x species. On the other hand, the H_2 consumption at 650 K is probably due to the reduction small palladium particles with strong interaction with the support [11].

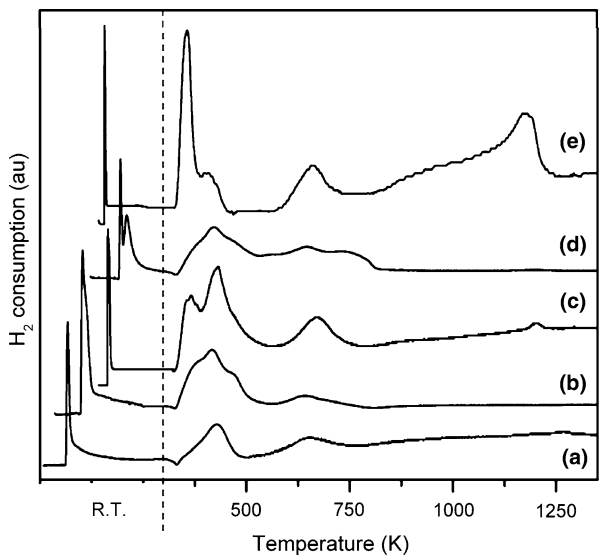

Fig. 2 TPR patterns of Pd/Al_2O_3 (**a**), Pd/6La–Al_2O_3 (**b**), Pd/6Ce–Al_2O_3 (**c**), Pd/12La–Al_2O_3 (**d**) and Pd/12Ce–Al_2O_3 (**e**)

The TPR profile of Pd/6La–Al_2O_3 is similar to the one obtained for Pd/Al_2O_3, with H_2 consumptions at room temperature, 440 and 650 K. However, it can be observed that the addition of lanthana caused the appearance of some differences on the reduction profile. There is an increase of the H_2 uptake at room temperature, the appearance of a shoulder around 480 K and an increase on the intensity of the peaks at high temperatures region, probably due to the interaction of palladium with some lanthana particles. The change of the lanthana content to 12 wt. % a reduction peak appeared, around 740 K, the H_2-comsuption is higher compared to the amount of PdO (Table 1), resulting in the H_2 consumption/PdO ratio higher than the stoichiometric. There are some controversies about how to assign the H_2 consumption at 740 K [10, 12–16] but several authors suggest that this peak may be related to the reduction of small quantities of La_2O_3 to LaO_x [10]. However, TPR experiments done with (x)La-Al_2O_3 supports (not showed) reveal that there is no H_2 consumption up to 1,273 K. Therefore, it could be suggested that this peak is due to the reduction of the lanthana support that supposedly is associate with the cleavage of the H–H bond on highly dispersed Pd^0 particles, which promote the reduction of the lanthana.

The TPR of Pd/xCe–Al_2O_3 samples show two peaks at high temperatures (630 and 1,140 K), two intermediate ones at around 350 and 400 K, in addition to the peaks at room temperature. Again, the peaks at room temperature may be assigned to the reduction of large palladium oxide particles [11]. The peak at around 400 K was also observed on Pd/Al_2O_3 catalyst and it was attributed to the reduction of small PdO particles deposited over alumina. The addition of ceria led to the appearance of the peak at 350 K. The change of ceria content from 6 to 12 wt.% caused the increase of the intensity of the peak at 350 K with a simultaneous decrease of the intensity of the peak at 400 K, and the Pd/12Ce–Al_2O_3 show a H_2 consumption/PdO ratio of 1.69. This peak is likely due to the reduction of PdO in interaction with CeO_2 and to the promoted reduction of ceria by the Pd^0 particles previously formed. The PdO in interaction with CeO_2 is the main species in the samples with higher CeO_2 loading. Monteiro et al. [17] also observed different interaction levels of PdO with the support on Pd/CeO_2/Al_2O_3 catalysts. They proposed that palladium particles were deposited over alumina and ceria depending on the ceria content and the preparation method. The peaks at 630 and 1,140 K were attributed to the formation of non-stoichiometric cerium oxides and Ce_2O_3, respectively [17].

XPS spectra of Pd $3d_{5/2}$ and Pd $3p_{3/2}$/O 1s regions for oxidized Pd/xLa–Al_2O_3, Pd/x Ce–Al_2O_3 samples are shown

in Fig. 3A, D, respectively. The Pd/6La–Al_2O_3, Pd/12 Ce–Al_2O_3 and Pd/12La–Al_2O_3 samples show a peak of Pd 3*d* and Pd $3p_{3/2}$ at about 336.7 ± 1 eV and 534.3 ± 2 eV, respectively. The peak position is characteristic of PdO according to the literature [18, 19]. Although Pd/Al_2O_3 and Pd/6Ce–Al_2O_3 samples shown a peak of Pd 3*d* at about 336.7 ± 1 eV, characteristic of PdO, the peak of Pd $3p_{3/2}$/O 1*s* is at 531.2 ± 2 eV and highly symmetric.

The XPS spectra of Ce 3*d* core electron levels for oxidized Pd/6Ce–Al_2O_3 and Pd/12Ce–Al_2O_3 samples are shown in Fig. 3B. In the spectra, there are six peaks corresponding to three pairs of spin-orbit doublets similar to spectrum of oxidized CeO_2 as previously described elsewhere [20, 21]. The $3d_{5/2}$ features at 881.8, 887.3 and 897.8 eV correspond to v , v^{II} and v^{III} components, respectively. The $3d_{3/2}$ features at 901, 905.4 and 915.9 eV correspond to u , u^{II} and u^{III} components, respectively. The v^{III} (u^{III}) and v (u) peaks are assigned to the final f^0 and f^1 state, respectively [22]. According to the literature the absence of the u^{III} peak can be interpreted as the lack of 4*p* configuration in the formal Ce^{3+} state and the percent area for the u^{III} peak in the total Ce 3*d* region (Ce $3d_{5/2}$ and Ce $3d_{3/2}$) correspond to the relative amount of Ce^{4+} in the sample [21]. The relative increase of percent area for the u^{III} area from 10 to 14% with increasing of Ce loading from 6 to 12 wt., respectively, indicates an increase of relative Ce^{+4} species with increase of Ce loading. Similar behavior was previously observed for Pt/*x*CeO_2–Al_2O_3 samples [8]. The samples with higher Ce loading Pd/12Ce–Al_2O_3 in the of Pd $3p_{3/2}$/O 1 *s* show an additional peak at 529.1 eV (Fig. 3D). This is related to a contribution of the oxygen from CeO_2 with fluorite structure [23].

The XPS spectra La $3d_{5/2}$ core electron levels for oxidized Pd/6La–Al_2O_3 and Pd/12La–Al_2O_3 samples are at 834.7 and 834.5 eV respectively (Fig. 3C) and are similar to that previously reported for La_2O_3 and dispersed Pd/La_2O_3 [24].

Figure 4 shows the FTIR spectra for CO adsorption on Pd/Al_2O_3, Pd/*x*Ce–Al_2O_3, Pd/*x*La–Al_2O_3 catalysts reduced at 773 K. The spectra present bands in two regions: in the high-frequency (HF) region (2,000–2,100 cm^{-1}) and low-frequency (LF) region (1,800–2,000 cm^{-1}). The spectrum of Pd/Al_2O_3 sample shows one HF band at 2,067 cm^{-1}, related to CO linearly bonded [25], and two LF bands at 1,959 and 1,900 cm^{-1} due to the compressed and isolated bridged carbonyls, respectively [26]. The band at HF shifted to lower frequency with the increase of CeO_2 or La_2O_3 loadings. For Pd/12Ce–Al_2O_3 and Pd/12La–Al_2O_3 samples there is a band around 2,050 cm^{-1}. The ratio of the bands (LF/HF) depends on the kind of support. The LF/HF ratio is around 5.2 for Pd/Al_2O_3 sample, and this ratio decreases with the increase of CeO_2 or La_2O_3 loadings. For

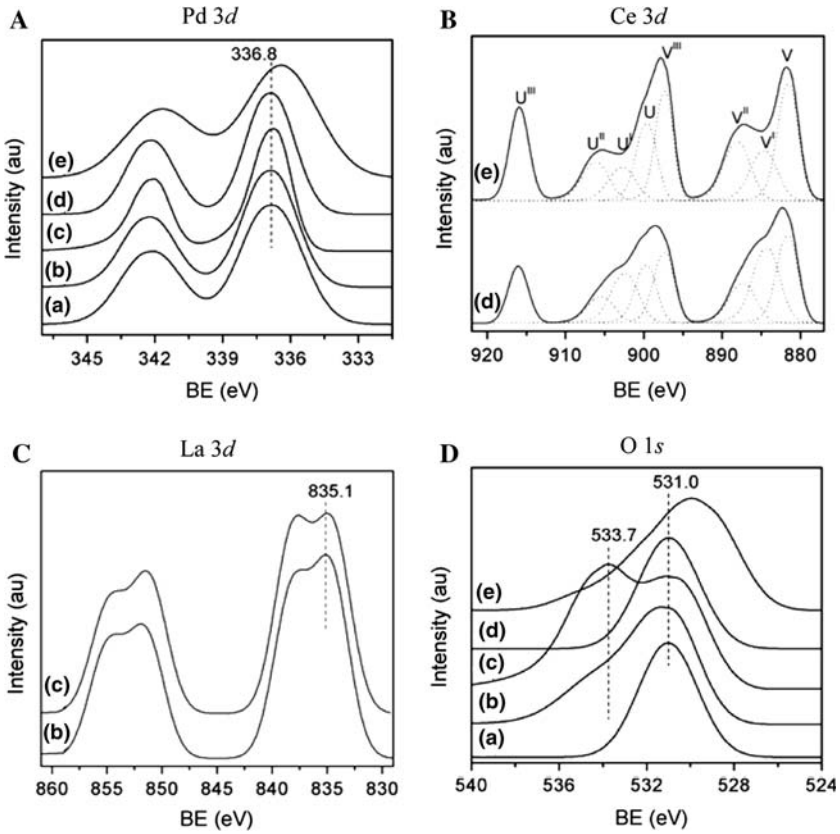

Fig. 3 (**A**) XPS of Pd 3*d* core levels; (**B**) XPS for Ce 3*d* core levels; (**C**) XPS for La 3*d* core levels and (**D**) XPS of O 1*s* core levels for oxide samples: (a) Pd/Al_2O_3, (b) Pd/6La–Al_2O_3, (c) Pd/12La–Al_2O_3, (d) Pd/6Ce–Al_2O_3 and (e) Pd/12Ce–Al_2O_3

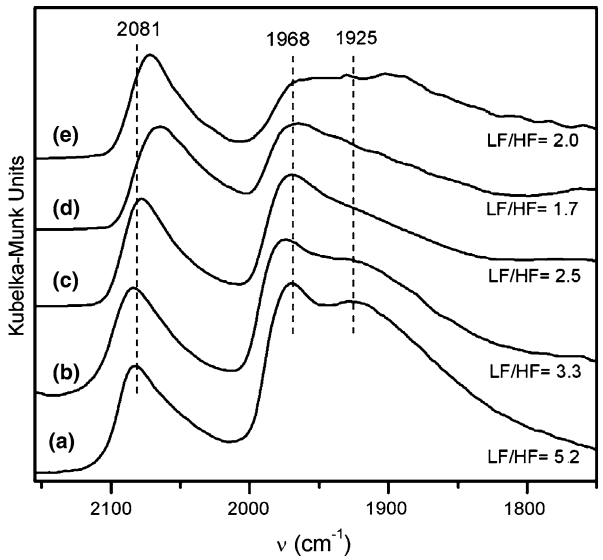

Fig. 4 FTIR spectra of CO adsorbed and ratios LF/HF of Pd/Al_2O_3 (a), $Pd/6Ce–Al_2O_3$ (b), $Pd/6La–Al_2O_3$ (c), $Pd/12Ce–Al_2O_3$ (d) and $Pd/12La–Al_2O_3$ (e)

the catalysts with 12 wt.% of CeO_2 or La_2O_3, the LF/HF ratio is 1.7 and 2.3, respectively.

The Arrhenius plots for steam reforming rates are presented in Fig. 5, the apparent activation energies are reported in Table 1. The joint confidence region of E_a^{ap} was about ± 0.5 kJ/mol for all catalysts. The obtained E_a^{ap} values for $Pd/xCe–Al_2O_3$ and $Pd/xLa–Al_2O_3$ catalysts are in the region 73–88 kJ mol^{-1} and these values agree with values previously reported for Pt, Rh, Ir catalyst in steam reforming of methane [1, 27–29]. The TOF_{CH4} values increase and E_a^{ap} decrease with increasing La_2O_3 and CeO_2 loadings. As previously demonstrated by Bradford and Vannice [30] an decrease of TOF_{CH4} followed by a decreasing of E_a^{ap} will be expected by presence of external mass transfer effects or by influence of water–gas-shift reactions. However our results show an increase of TOF_{CH4} followed by a decreasing of E_a^{ap}, which cannot be connected with a possible presence of external mass transfer effects or influence of water–gas-shift reactions. Interestingly, the $Pd/12Ce–Al_2O_3$ catalysts show Pd dispersions of 22%, which are lower than that of Pd/Al_2O_3 (40%) and TOF_{CH4} for $Pd/12Ce–Al_2O_3$ catalysts are higher, compared to that of Pd/Al_2O_3 catalyst. Although the $Pd/12La–Al_2O_3$ catalysts show Pd dispersions (43%) similar to the one of Pd/Al_2O_3 (40%), the TOF_{CH4} for $Pd/12La–Al_2O_3$ catalysts is higher. This suggests that the activity for steam reforming of methane is promoted by addition of ceria or lanthana on Al_2O_3 support.

The values of E_a^{ap} dropped around 20 kJ/mol for the samples containing 12 wt.% of ceria or lanthana. This change in the E_a^{ap} can be considered significant for the methane steam reforming reaction and it suggests that the increase of ceria or lanthana content increases the activity of the sites. Although there is a decrease of the palladium dispersions with the increase of ceria or lanthana content, the boost in the activity is sufficient to overcome the decrease of the number of active sites and still lead to an increase of the specific reaction rate. A increasing of activity with an increase of the metal dispersion is found in the literature for this reaction using Ni [1], Rh [27] and Pt [28] catalysts.

A graphic of the intensities ratio of the HF/LF bands versus Turnover Frequency (TOF_{CH4}) for steam reforming of methane is presented in Fig. 6. Although the bands at LF

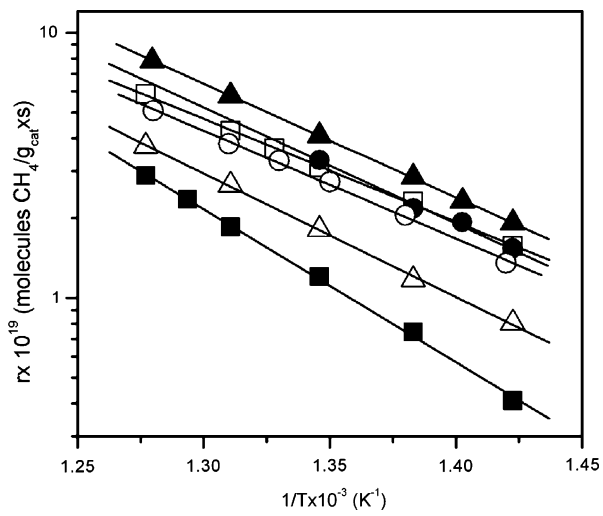

Fig. 5 Arrhenius plots for steam reforming of CH_4 on Pd/Al_2O_3 (■), $Pd/6La–Al_2O_3$ (●), $Pd/12La–Al_2O_3$ (▲), $Pd/3Ce–Al_2O_3$ (△), $Pd/6Ce–Al_2O_3$ (◯) and $Pd/12Ce–Al_2O_3$ (□)

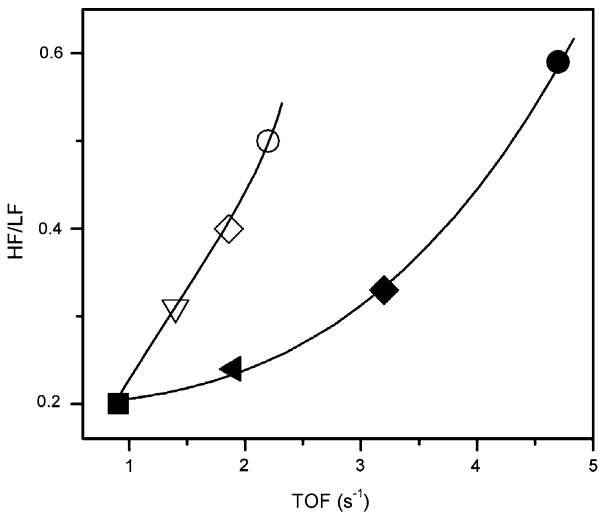

Fig. 6 The HF/LF ratio as a function of TOF_{CH4} for SRM at 783 K Pd/Al_2O_3 (■), $Pd/1La–Al_2O_3$ (▽), $Pd/6La–Al_2O_3$ (◇), $Pd/12La–Al_2O_3$ (◯), $Pd/3Ce–Al_2O_3$ (◀), $Pd/6Ce–Al_2O_3$ (♦) and $Pd/12Ce–Al_2O_3$ (●)

region are strongly suppressed in Pd/12Ce–Al_2O_3 and Pd/12La–Al_2O_3 catalysts, resulting in lower accuracy of HF/LF ratio, there is a distinct correlation between the increase of TOF_{CH4} with the increase of HF/LF ratio for ceria and lanthana promoted catalysts series. These results show clearly that for similar changes on relative CO adsorption mode (HF/LF), the ceria promoted catalysts series are more effective than lanthana to increase the catalytic activity, while the higher Pd dispersion in La catalysts series became the lanthana promoted catalysts with higher specific reaction rate (Fig. 5).

4 Discussion

For monometallic catalysts, the LF/HF ratio can be correlated to Pd dispersion as Sheu et al. demonstrated for Pd/SiO_2 catalysts [31]. The LF/HF ratio decreases with increasing Pd dispersion, considering that isolated sites and protruding atoms in corner or edge positions are more efficient than terrace sites to CO adsorption in linear form. Then, the LF/HF ratio can be correlated to the ratio between the numbers of high and low coordination sites on Pd surface. Therefore, a decrease of LF/HF ratio can be expected with an increase of the Pd dispersion. This behavior is verified only for sample with lower La-containing (1 wt. % of lanthana) in comparison with Pd/Al_2O_3 catalyst, which shows a decrease of LF/HF ratio with increase of Pd dispersion (Table 1). Interestingly, the inverse was observed for the samples in the present study with high Ce- or La-contents. Pd/Al_2O_3 catalyst with Pd dispersion of 40% show higher LF/HF ratio, while Pd/12Ce–Al_2O_3 sample with lower Pd dispersion of 23% exhibit lower LF/HF ratio. The Pd/12La–Al_2O_3 catalyst, which has similar dispersion to Pd/Al_2O_3, shows a lower LF/HF ratio. This phenomenon could be connected with the formation of an adduct MPd_xO (M = Ce or La) at the surface of the metal crystallites in Pd/12Ce–Al_2O_3 and Pd/12La–Al_2O_3 catalysts, similar to previously proposed by Fleisch at al. [24] for palladium supported on La_2O_3. It is possible that the presence of CeO_x or LaO_x species on the Pd surface could cause a decrease of cyclohexanés accessibility. Therefore, when the Pd dispersion is calculated from the rate of dehydrogenation of cyclohexane, a decrease of dispersion is observed, and it is expected that CO adsorption in bridge carbonyl form is more hindered due to geometric effects.

When CeO_2 and La_2O_3 loadings increase, the bands in HF shift to lower frequency relative to Pd/Al_2O_3 catalyst. This shift can be attributed to dipole–dipole effect the position of this band is strongly coverage-dependent on Pd catalysts [32]. On the other hand, the band in LF region does not shift significantly by the decrease of CO coverage during the CO desorption. Then, the shift of the band relative to CO adsorbed in linear form to lower frequency may be occurring due to an increase of electron-density on the Pd surface and to the geometric effect caused by CeO_x or LaO_x species on the Pd surface. Although, it is worth noting that the surface reconstruction can be occurring due to CO adsorption, in the Pd case it is not conclusive. Nevertheless, one may consider that in reaction where CO is a product, as the case of steam reforming of methane, the possible morphology changes by the CO may be relevant to the reaction mechanism.

Activation of methane studies suggested that the activation of C–H bond is sensitive to the metal structure on the catalyst surface. The decrease of metal particle size increases the activity of the metal sites. In other words, the metal sites with lower coordination number are more active than terrace sites [33]. Wei and Iglesia [27, 28, 34] performed several kinetic studies using isotopic exchange of CH_4 and CD_4 on Pt, Ir, Rh, Ru catalysts supported on ZrO_2, γ-Al_2O_3 and ZrO_2–CeO_2. They showed that the rate limiting step of methane reforming with CO_2 and H_2O is the cleavage of the C–H bond, which occurs only on the metal surface and it is not affected by the presence of CO_2 or H_2O. The authors also showed an increase of TOF_{CH4} values for the steam reforming of methane reaction with the increase of metal dispersions for Pt, Rh, Ru and Ir catalysts regardless of the support nature.

The changes observed on the reaction rate, E_a^{ap} and TOF_{CH4} values may be related to structure modifications of the superficial palladium caused by the addition of ceria and lanthana. The DRIFTS results showed the suppression on the amount of CO adsorbed with the increase of lanthana or ceria contents, suggesting a decrease on the number of exposed palladium sites. This result agrees well with the palladium dispersions determined by the dehydrogenation of cyclohexane. The DRIFTS data also suggested that the increase of the ceria or lanthana contents caused an increase of the fraction of low coordination sites (defects), with a consequent decrease of the fraction of high coordination sites (terraces). According to Sheu et al. [31], an increase of HF/LF ratio of Pd/SiO_2 samples is related to an increase of the palladium dispersion. However, our results for Pd/Ce–Al_2O_3 and Pd/La–Al_2O_3 catalysts with high ceria or lanthana loading showed a decrease of the palladium dispersion with the increase of the HF/LF ratio. This could be related to the partial coverage of Pd sites by ceria or lanthana species. These results also suggest that CeO_x or LaO_x species would cover terrace Pd sites and due to a geometric effect suppress the CO adsorption in the bridge form. Considering that terrace sites have lower electronic density [35] and therefore are less active for the methane steam reaction when compared with defective sites, it is reasonable to observe an increase of the

TOF_{CH4} and of the specific reaction rate and a decrease of the E_a^{ap} with the raise of ceria or lanthana content.

In order to understand better the rise of the catalytic activity coupled with the decrease of the palladium dispersion in Pd/Ce–Al_2O_3 and Pd/La–Al_2O_3 catalysts with high ceria or lanthana loading, one should consider the reaction mechanism [1]. Several authors [36–38] propose that besides the reform reaction, there are parallel reactions such as methane and CO decomposition leading to the formation of carbon on the surface. This carbon (C*) may react with oxygen species (O*) on the metal surface leading to CO or form more stable carbon structures that would deactivate the catalyst. On the other hand, Wei and Iglesia [1, 27, 28, 34] proposed that the formation of carbon on the surface may occur by two different routes: (i) methane decomposition through different dissociation steps until the formation of C* and (ii) CO disproportionation forming C* and CO_2. The concentration of C* on the surface will be a function of the experimental conditions such as temperature, of CH_4 and H_2O concentrations, which are the precursors of the C* and O* species, and also of the specific reaction rate between C* and O*.

From this information, it is reasonable to suppose that a partial blockage of Pd sites by ceria or lanthana could result on an increase of TOF_{CH4} and specific reaction rates values only if there was a smaller accumulation of carbon on the active sites. However, the literature data suggest that an increase of electronic density of the metal favors the methane activation. In this case, the decrease of the electronic density should disfavor the methane activation, and therefore, would not lead to an increase of the catalytic activity. Alternatively, it is expected that the partial coverage of Pd^0 by ceria or lanthana species could lead to the formation of an adduct MPd_xO (M = Ce or La) at the surface of the metal crystallites and at Pd^0*$Pd^{\delta+}$O–M interfaces the CH_4 molecule can be polarized as H_3–C–H–$OPd^{\delta+}$ and promoted the activation of CH_4 on Pd surface (H_xC–Pd^0). Similar mechanism was previously proposed for the activation of CH_4 during the oxidation of methane on Pd–PdO surface [39]. On the other hand, the Pd^0*$Pd^{\delta+}$O–M interfacial species (M = Ce or La) could be oxidized by H_2O or CO_2, promoting the O* transfer to the metal surface. This could facilitate the removal of C* species from the metal surface. For Pd/12Ce–Al_2O_3 catalysts, the XPS show a O 1*s* binding energies higher at 529.1 eV, related to a contribution of the oxygen from CeO_2 with fluorite structure, which can correlated with oxygen reversible exchanged, called oxygen storage capacity. This effect can intensify the O* transfer to the metal and oxidize de C* at Pd surface, resulting in the increase of the activity with the increase of ceria loading higher than Pd/*x*La–Al_2O_3 catalysts. Pd sites with high coordination are partially blocked, which decreases the susceptibility to C* formation by CO disproporcionation. Conversely, the sites with lower coordination are exposed to the transfer of O* from the ceria with fluorite structure to Pd surface and the C* is removed from Pd surface. Consequently, the accessibility of the very active sites to CH_4 activation and TOF_{CH4} increase with raising CeO_2 loadings.

The partial coverage of Pd surface by ceria or lanthana species promote several different effects: (i) partial coverage of Pd sites; (ii) increase of the fraction of Pd sites with higher electronic density; and (iii) transfer of O* species to the Pd surface, which would promote the removal of C* adsorbed on the Pd sites with higher electronic density and more active for the activation of methane.

5 Conclusions

The increase of the activity of the Pd/*x*La–Al_2O_3 and Pd/*x*Ce–Al_2O_3 catalysts was attributed to various effects of CeO_2 and La_2O_3 such as: (i) change of superficial Pd structure with blockage of Pd sites by CeO_2 and La_2O_3; (ii) the Pd^0*$Pd^{\delta+}$O–M interfacial species (M = Ce or La) are oxidized by H_2O or CO_2, promoting the O* transfer to the metal surface, which can decrease the carbon formation on Pd surface. Considering that these effects of CeO_2 and La_2O_3 are opposite to changes of the reaction rate, the increase of specific reaction rate with the Ce and La loading suggests that net effect results in the increase of the accessibility of CH_4 to metal active sites in Pd/12La/Al_2O_3 or Pd/12Ce/Al_2O_3 catalysts.

Acknowledgments The authors are grateful for the financial support of CNPq (Conselho Nacional de Desenvolvimento científico e Tecnológico) and CAPES (Coordenação de Aperfeiçoamento de Pessoal de Nível Superior. Pascal Bargiela from Instituto de Química/Instituto de Física-Nuclear da UFBA- Universidade Federal da Bahia that assisted in collecting XPS data.

References

1. Wei J, Iglesia E (2004) JCatal 224:370
2. Larsen JH (1999) Ib Chorkendorff Surf Sci Reports 35:163
3. Bengaard HS, Norskov JK, Sehested J, Clausen BS, Nielsen LP, Molenbroek AM, Rostrup-Nielsen JR (2002) J Catal 209:365
4. Zhang X, Walters AB, Vannice MA (1995) J Catal 155:290
5. Guiner A (1994) X-ray diffraction in crystals, imperfect crystals and amorphous bodies. Dover Publications, New York
6. Rogemond E, Essayem N, Frety R, Perrichon V, Primet M, Mathis F (1997) J Catal 166:229
7. González-Marcos MP, Iñarra B, Guil JM, Gutiérrez-Ortiz MA (2004) App Catal A: Gen 273:259
8. Damyanova S, Bueno JMC (2003) Appl Catal A: Gen 253:135
9. Feio LSF, Hori CE, Damyanova S, Noronha FB, Cassinelli WH, Marques CMP, Bueno JMC (2007) Appl Catal A: Gen 316:107

10. Barrera A, Viniegra M, Bosch P, Lara VH, Fuentes S (2001) Appl Catal B 34:97
11. Lieske H, Völter J (1985) J Phys Chem 89:1841
12. Barrera A, Viniegra M, Fuentes S, Diaz G (2005) Appl Catal B 56:279
13. Bogdanchikova NE, Fuentes S, Borja MA, Farías MH, Boronin A, Diaz G (1998) Appl Catal B 17:221
14. Fuentes S, Bogdanchikova NE, Borja MA, Boronin A, Farias MH, Diaz G, Cortes AG, Barrera A (2000) Catal Today 55:301
15. Fuentes S, Bogdanchikova NE, Diaz G, Peraza M, Sandoval GC (1997) Catal Lett 47:27
16. Hoost TE, Otto K (1992) Appl Catal A: Gen 92:39
17. Monteiro RS, Noronha FB, Dieguez LC, Schmal M (1995) Appl Catal A: Gen 131:89
18. Monteiro RS, Zemlyanov D, Storey JM, Ribeiro FH (2001) J Catal 199:291
19. Haack LP, Otto K (1995) Catal Lett 34:31
20. Riguetto BA, Damyanova S, Gouliev G, Marques CMP, Petrov A, Bueno JMC (2004) J Phys Chem B 108:5349
21. Shyu JZ, Weber WH, Gandhi HS (1988) J Phys Chem 92:4964
22. Fujimori A (1983) Phys Rev B 27:3992
23. Damyanova S, Perez CA, Schmal M, Bueno JMC (2002) Appl Catal A 234:271
24. Fleisch TH, Hicks RF, Bell AT (1984) J Catal 87:398
25. Craciun R, Daniell W, Knözinger H (2002) Appl Catal A 230:153
26. Tessier D, Rakai A, Bozon-Verduraz F (1992) J Chem Soc Faraday Trans 88:741
27. Wei J, Iglesia E (2004) J Catal 225:116
28. Wei J, Iglesia E (2004) J Phys Chem B 108:4098
29. Wei J, Iglesia E (2004) Phys Chem Chem Phys 6:3754
30. Bradford MCJ, Vannice MA (1999) J Catal 183:69
31. Sheu LL, Karpinksi Z, Sachtler WMH (1989) J Phys Chem 93:4890
32. Hollins P (1992) Surf Sci Rep 16:54
33. Anderson AB, Maloney J (1988) J Phys Chem 92:809
34. Wei J, Iglesia E (2004) J Phys Chem B 108:7253
35. Blyholder G (1964) J Phys Chem 68:2772
36. Trimm DL (1997) Catal Today 37:233
37. Trimm DL (1999) Catal Today 49:3
38. Xu J, Froment GF (1989) Iech J 35:83
39. Fujimoto K, Ribeiro FH, Avalos-Borja M, Iglesia E (1998) J Catal 179:431